

JOURNAL OF GLACIOLOGY



CAMBRIDGE
UNIVERSITY PRESS

THIS MANUSCRIPT HAS BEEN SUBMITTED TO THE JOURNAL OF GLACIOLOGY AND HAS NOT BEEN PEER-REVIEWED.

Melting temperature changes during slip across subglacial cavities drive basal mass exchange

Journal:	<i>Journal of Glaciology</i>
Manuscript ID	JOG-21-0025.R1
Manuscript Type:	Letter
Date Submitted by the Author:	n/a
Complete List of Authors:	Rempel, Alan; University of Oregon, Earth Sciences Meyer, Colin; Dartmouth College, Thayer School of Engineering Riverman, Kiya; University of Oregon, Earth Science
Keywords:	Basal ice, Ice physics, Melt - basal, Subglacial processes
Abstract:	The importance of glacier sliding has motivated a rich literature describing the thermomechanical interactions between ice, liquid water, and bed materials. Early recognition of the gradient in melting temperature across small bed obstacles led to focussed studies of regelation. An appreciation for the limits on ice deformation rates downstream of larger obstacles highlighted a role for cavitation, which has subsequently gained prominence in descriptions of subglacial drainage. Here, we show that the changes in melting temperature that accompany changes in normal stress along a sliding ice interface near cavities and other macroscopic drainage elements cause appreciable supercooling and basal mass exchange. This provides the basis of a novel formation mechanism for widely observed laminated debris-rich

	basal ice layers.

SCHOLARONE™
Manuscripts

Melting temperature changes during slip across subglacial cavities drive basal mass exchange

Alan W. REMPEL,¹ Colin R. MEYER,² Kiya L. RIVERMAN¹

¹*Department of Earth Sciences, University of Oregon, Eugene, OR, USA*

²*Thayer School of Engineering, Dartmouth College, Hanover, NH, USA*

Correspondence: Alan Rempel <rempel@uoregon.edu>

ABSTRACT. The importance of glacier sliding has motivated a rich literature describing the thermomechanical interactions between ice, liquid water, and bed materials. Early recognition of the gradient in melting temperature across small bed obstacles led to focussed studies of regelation. An appreciation for the limits on ice deformation rates downstream of larger obstacles highlighted a role for cavitation, which has subsequently gained prominence in descriptions of subglacial drainage. Here, we show that the changes in melting temperature that accompany changes in normal stress along a sliding ice interface near cavities and other macroscopic drainage elements cause appreciable supercooling and basal mass exchange. This provides the basis of a novel formation mechanism for widely observed laminated debris-rich basal ice layers.

INTRODUCTION

At an ice–liquid interface, the dependence of melting temperature on normal stress drives ice regelation (e.g. Bottomley, 1872; Drake and Shreve, 1973; Gilpin, 1979; Nye, 1967; Rempel and Meyer, 2019; Telford and Turner, 1963). Regelation facilitates glacier sliding by causing ice to melt on the upstream sides of small bumps, where elevated normal stresses lower the melting temperature, and subsequently refreeze on their

Table 1. List of symbols, in alphabetical order, with Greek letters below (value of physical constant in parentheses).

A	softness parameter in flow law ($6.8 \times 10^{-24} \text{ s}^{-1} \text{ Pa}^{-n}$)
A	element of horizontally projected basal area
C_0	Clapeyron slope ($7.4 \times 10^{-8} \text{ K Pa}^{-1}$)
C_p	heat capacity of ice ($2.1 \times 10^3 \text{ J kg}^{-1} \text{ K}^{-1}$)
d	obstacle height
g	acceleration of gravity (9.8 m s^{-2})
h	ice-equivalent freeze-on thickness
h_0	ice-equivalent freeze-on thickness added over one cavity
h_{\min}	ice-equivalent freeze-on thickness immediately upstream of cavities
h_{\max}	ice-equivalent freeze-on thickness immediately downstream of cavities
H	ice-equivalent glacier thickness
H_0	average ice-equivalent glacier thickness
j	index variable
J	number of complete unload/reload cycles
ℓ	along-slip cavity dimension
\mathcal{L}	latent heat of fusion ($3.3 \times 10^5 \text{ J kg}^{-1}$)
n	Glen's flow law exponent (3)
N	effective stress: $\rho_i g H_0 - P$
P_0	reference pressure – chosen as average overburden pressure: $\rho_i g H_0$
P	liquid pressure
P_T	thermomolecular pressure supported by ice–mineral forces: $\sigma_n - P$
t	time
T	temperature
T_{eq}	equilibrium temperature
T_{drainage}	equilibrium temperature over drainage elements
T_{premelt}	equilibrium temperature outside drainage elements
T_0	reference temperature – equilibrium temperature at $\sigma_n = P = P_0$
ΔT	temperature difference $T_{\text{drainage}} - T_{\text{premelt}}$
u_s	sliding velocity
v	creep closure rate
x	slip distance
κ	thermal diffusivity of ice ($1.2 \times 10^{-6} \text{ m}^2 \text{ s}^{-1}$)
ϕ	drainage area fraction
ϕ_0	reference drainage area fraction
σ_n	spatially varying normal stress at basal ice surface
ρ_l	liquid density (10^3 kg m^{-3})
ρ_i	ice density ($9.2 \times 10^2 \text{ kg m}^{-3}$)

24 downstream sides, where reduced normal stresses increase the melting temperature. Larger bed obstacles
25 are surmounted more easily by ice deformation, and the combination of processes is parameterized in well-
26 known sliding laws (e.g. Kamb, 1970; Nye, 1969; Weertman, 1957). An important complication develops
27 when sliding transports ice more rapidly than deformation enables it to conform to the shapes of rough beds.
28 In these locations, cavities develop and fill with pressurized meltwater (e.g. Fowler, 2010; Lliboutry, 1968;
29 Schoof, 2005). Links between cavities enable water flow, making them important for subglacial drainage
30 (e.g. Flowers, 2015; Kamb, 1987). Cavity formation is also associated with heterogeneity in the normal
31 stress exerted on the basal ice interface, since the liquid pressure is typically lower than the ice overburden
32 pressure (e.g. Iken and Bindschadler, 1986) and higher bridging stresses must support the remaining glacier
33 weight. Such bridging stresses can be generated by intermolecular interactions between mineral (i.e. rock
34 or till) and ice surfaces across microscopic premelted liquid films (Dash and others, 2006; Rempel, 2008;
35 Rempel and Meyer, 2019). Whereas conventional regelation sliding, described first by Weertman (1957),
36 relies on the steady conductive heat transfer that accompanies melting temperature contrasts as ice slides
37 across bedrock bumps, our attention is drawn to consider transient phase change processes promoted by
38 conductive heat transfer between the basal interface and overlying ice.

39 Here, we explore the consequences of changes in melting temperature that are caused by stress
40 heterogeneities along the basal interface. We focus on the freezing that is induced as ice slides from regions
41 of elevated normal stress, supported in part by ice–mineral interactions, onto regions of reduced normal
42 stress balanced solely by the liquid pressure. Such transitions are expected as slip transports ice over
43 macroscopic drainage elements (e.g. cavities), and as macroscopic drainage elements incised upwards into
44 the ice (e.g. R-channels) are dragged across newly unloaded mineral exposures. We find that a simple model
45 for ice–liquid exchange in a sliding regime predicts freeze-on thicknesses that are consistent with diverse
46 basal observations. Where this freeze-on occurs in the presence of unconsolidated or suspended sediments,
47 debris bands in basal ice can form. We suggest that mm-scale diffuse and sometimes laminated debris bands
48 that are preserved in basal ice layers (e.g. Hubbard and others, 2009; Knight, 1997; Sugden and others,
49 1987) may represent the signatures of the freeze-on processes that we describe. This is noteworthy because
50 the properties of basal ice, including the presence and concentration of entrained debris, can influence
51 sliding behavior and erosion (e.g. Thompson and others, 2020).

52 BASAL PHASE BEHAVIOR – BULK MELTING AND PREMELTING

53 For pure water, the equilibrium temperature at an ice–liquid interface is determined to leading order by
 54 the pressure in the liquid P and the normal stress exerted on the solid ice surface σ_n ; under typical
 55 glaciological conditions, the other components of the ice stress tensor at the interface contribute negligibly.
 56 The thermodynamic arguments leading to this result are given by a number of sources (e.g. Kamb, 1961;
 57 Paterson, 1973; Sekerka and Cahn, 2004). The offset of the equilibrium temperature T_{eq} from a constant
 58 reference temperature T_0 can be written as (c.f. Rempel, 2008, Eq. 1)

$$T_{\text{eq}} - T_0 \approx -C_0 \left[P - P_0 + \frac{\rho_l}{\rho_l - \rho_i} (\sigma_n - P) \right], \quad (1)$$

59 where P_0 is the constant reference pressure (defined so that $T_{\text{eq}} = T_0$ when $P = \sigma_n = P_0$), ρ_l and ρ_i are
 60 the densities of liquid water and ice, and the magnitude of the Clapeyron slope is

$$C_0 = T_0 \frac{\rho_l - \rho_i}{\rho_l \rho_i \mathcal{L}} \approx 7.4 \times 10^{-8} \text{ K/Pa}, \quad (2)$$

61 where \mathcal{L} is the latent heat of fusion (a list of symbols is given in Table 1). An expanded discussion of
 62 equilibrium melting conditions is provided in the Supplementary Information.

63 Along an interface between ice and a macroscopic drainage element like a cavity or channel, the normal
 64 stress in the ice balances the liquid pressure (i.e. $\sigma_n = P$, see Fig. 1). Hence, along the ice-walled surfaces
 65 of macroscopic drainage elements, the final term in equation (1) vanishes and variations in the melting
 66 temperature are directly proportional to variations in liquid pressure, decreasing by approximately 7.4 mK
 67 for each atmosphere ($\sim 10^5$ Pa) increase in P . More generally, the intermolecular forces that cause premelted
 68 liquid films to separate ice from mineral surfaces (i.e. bedrock and/or unconsolidated sediments) produce a
 69 difference between the normal stress σ_n and the liquid pressure P that is referred to as the thermomolecular,
 70 or disjoining, pressure (e.g. Dash, 1989; Dash and others, 2006; Wettlaufer and Worster, 2006). A significant
 71 literature has developed to describe the molecular scale mechanisms that facilitate stress transfer between
 72 solid surfaces across intervening premelted films (e.g. Dash and others, 2006; Israelachvili, 2011), but for
 73 our purposes it suffices to note that all of these mechanisms produce the same essential result. When
 74 homogenized over an area element of the (generally rough) glacier bed, the thermomolecular pressure,
 75 defined here as $P_T = \sigma_n - P$, is the component of ice normal stress supported by intermolecular interactions
 76 with mineral surfaces (discussed further in the Supplementary Information). As expressed by equation (1),
 77 changes in T_{eq} with P_T at constant P are an order of magnitude larger (i.e. $\rho_l/(\rho_l - \rho_i) \approx 12$) than changes

78 in T_{eq} with changes in P of the same size during which P_T is held constant (i.e. along a path with $\sigma_n = P$;
79 discussed further in the Supplementary Information).

80 Consider the idealized case of a glacier with ice-equivalent thickness H sliding over a heterogeneous bed
81 that contains macroscopic drainage elements with $P_T = 0$ (Figure 1). For basal areas \mathcal{A} over which the
82 glacier weight can be regarded as locally supported (i.e. shear stresses on the boundaries of \mathcal{A} are assumed
83 to contribute negligibly), the vertical force balance requires

$$\int_{\mathcal{A}} \rho_i g H \, d\mathcal{A} = \int_{\mathcal{A}} \sigma_n \, d\mathcal{A} = \int_{\mathcal{A}} (P + P_T) \, d\mathcal{A} . \quad (3)$$

84 (As discussed further in the Supplementary Information, the basal surface itself is generally expected to
85 be rough, and measurements of its physical area hence depend on the scale at which its topography is
86 resolved; in the integral expressions used here for evaluating the vertical force balance, the area element
87 $d\mathcal{A}$ is rigorously defined as the horizontal projection of the contorted basal surface, making it independent
88 of the scale of observation.) We assume that: (i) liquid wets the entire basal interface (consistent with our
89 focus on sliding glaciers), (ii) spatial variations in liquid pressure are small (i.e. the bed is ‘well-drained’),
90 (iii) macroscopic drainage elements occupy fractional bed area ϕ , and (iv) the thermomolecular pressure is
91 uniform over the remainder of the bed where ice–mineral separation diminishes enough that intermolecular
92 forces between them are significant (what we refer to as premelted films throughout). For an average ice-
93 equivalent thickness H_0 , under these idealized conditions equation (3) simplifies to (see the Supplementary
94 Information)

$$\rho_i g H_0 = P + (1 - \phi) P_T , \quad (4)$$

95 which indicates that, for basal areas \mathcal{A} over which the glacier weight is locally supported, part of that
96 weight is supported by the liquid pressure acting everywhere, and the remainder is supported by the
97 thermomolecular pressure acting on the fraction of the bed that is not occupied by macroscopic drainage
98 elements. Assigning the reference pressure as the average overburden $P_0 = \rho_i g H_0$, equation (1) implies that
99 the equilibrium melting temperature over the macroscopic drainage elements is

$$T_{\text{drainage}} = T_0 + C_0 N , \quad (5)$$

100 where the effective stress is defined as $N = \rho_i g H_0 - P$. Over the remainder of the bed, where stress
101 transfer takes place between the ice and mineral surfaces (i.e. the ice–mineral separation is reduced to the

102 microscopic dimensions of premelted liquid films), the equilibrium temperature is

$$T_{\text{premelt}} = T_{\text{drainage}} - \frac{C_0}{1 - \phi} \frac{\rho_l}{\rho_l - \rho_i} N. \quad (6)$$

103 Hence, the difference between the equilibrium ice–liquid temperature over a drainage element and that
104 over premelted regions is

$$\Delta T = \frac{C_0}{1 - \phi} \frac{\rho_l}{\rho_l - \rho_i} N. \quad (7)$$

105 When ϕ is vanishingly small, ΔT increases by approximately 90 mK (i.e. $7.4 \text{ mK} \times 12$) for each atmosphere
106 ($\sim 10^5 \text{ Pa}$) increase in the effective pressure N , or nearly $1^\circ\text{C}/\text{MPa}$.

107 BASAL MASS EXCHANGE

108 Freeze-on Over a Single Cavity

109 Having established that appreciable differences in equilibrium temperature can be expected across the
110 borders of drainage elements, we next examine the effects of these differences on basal mass exchange. For
111 a simple illustration, we consider a scenario in which ice slides over its bed at constant effective stress N
112 and constant velocity u_s (see Fig. 1). Treating the heat flow as perpendicular to the bed, with thermal
113 diffusivity κ , and assuming that phase changes are sufficiently slow that their effects on thermal conditions
114 can be neglected (i.e. bed-perpendicular advective heat transport is negligible), energy conservation is
115 governed by the one dimensional heat equation with an interface temperature that changes abruptly by
116 ΔT as the boundary of a drainage element is crossed at time $t = 0$. The resulting perturbation to the
117 temperature gradient along the sliding interface can be approximated as (e.g. Carslaw and Jaeger, 1959,
118 §2.5; discussed further in the Supplementary Information)

$$\nabla T \approx -\frac{\Delta T}{\sqrt{\pi \kappa t}}, \quad (8)$$

119 where the adopted sign convention signals that the heat flow upwards, away from the bed, increases when
120 the equilibrium temperature across the drainage element boundary rises by ΔT . Noting that $dx = u_s dt$ and
121 integrating over a sliding distance $\ell = u_s t$, the implied perturbation to conductive heat transport equates
122 with the latent heat of fusion for a layer of ice-equivalent thickness

$$h_0 = \int_0^\ell -\frac{C_p \kappa \nabla T}{u_s \mathcal{L}} dx = \frac{2}{\sqrt{\pi}} \ell \frac{C_p \Delta T}{\mathcal{L}} \sqrt{\frac{\kappa}{u_s \ell}}, \quad (9)$$

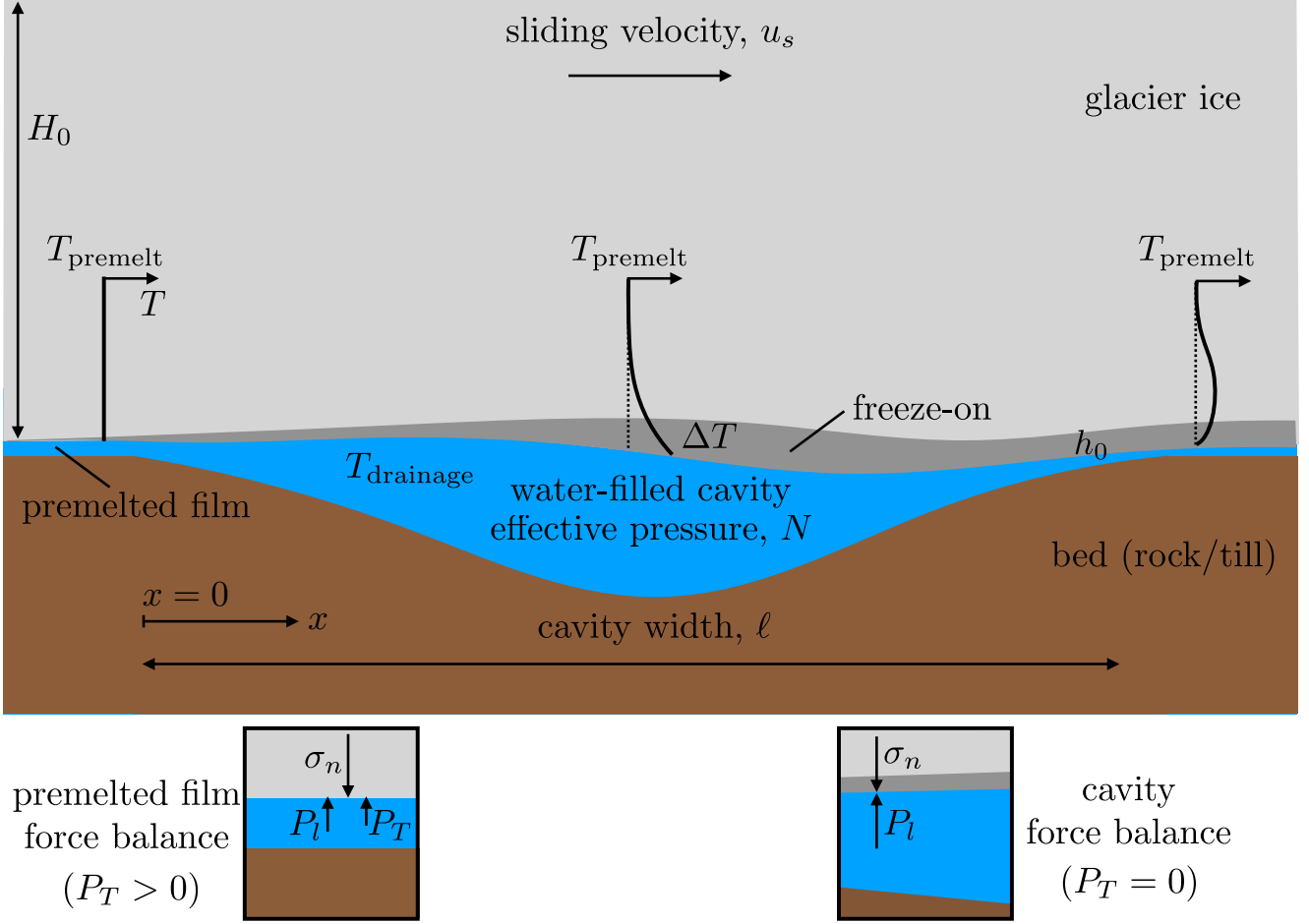


Fig. 1. Schematic of a representative cavity, with uniform liquid temperature $T_{\text{drainage}} = T_{\text{pre melt}} + \Delta T$, connected to premelted films that separate the bounding rock/till interface from the overlying glacier ice. Representative temperature profiles are shown (left to right): i) at the upstream side of the cavity prior to unloading (constant at $T_{\text{pre melt}}$), ii) midway over the cavity with a conductive profile promoting freeze-on (decaying from T_{drainage} to $T_{\text{pre melt}}$ far above the bed), and iii) at the downstream side of the cavity after the interface temperature has returned to $T_{\text{pre melt}}$ and melting has commenced (note the dissipating thermal wave above the bed). Note that the melt rate at iii is lower than the freezing rate at ii, promoting net freeze-on as ice flows across the schematic. Lower schematics show the force balance in the premelted film (left; $P_T > 0$) and in the cavity (right; $P_T = 0$).

123 where C_p is the heat capacity, and we note that the ratio of h_0 to a characteristic cavity size ℓ is inversely
 124 proportional to the product of the Stefan number $S_T = \mathcal{L}/(C_p \Delta T)$ with the square root of a Peclet number
 125 $P_e = u_s \ell / \kappa$. The energy transport needed to accommodate this phase change is dissipated by conduction
 126 into the overlying ice, which retains the thermal signature of having recently been adjacent to colder
 127 premelted basal regions.

Equation (9) indicates that for a given cavity size ℓ , the thickness h_0 is greater if the sliding speed is lower because there is more time for conductive heat transport. Freeze-on layer thickness is also greater if the effective stress is higher, which promotes elevated ΔT through equation (7). For intuition, at typical glacial sliding velocities u_s ranging between 10 m/a and 10^3 m/a, with ΔT between 0.1°C and 1°C (N between 10^5 Pa and 10^6 Pa), the freeze-on layer grows to achieve ice-equivalent thicknesses between $h_0 \approx 0.1$ mm (large u_s , small ΔT and N) and $h_0 \approx 10$ mm (small u_s , large ΔT and N) during the time taken to traverse a cavity of dimension $\ell = 1$ m. However, we note that the characteristic sizes ℓ of drainage elements need not be fixed, often increasing with sliding speed and decreasing with effective stress. A simple, illustrative model for cavity size that displays this qualitative behavior can be constructed using Glen's flow law with softness $A \approx 6.8 \times 10^{-24} \text{ s}^{-1} \text{ Pa}^{-n}$ (Cuffey and Paterson, 2010) to estimate a characteristic creep rate (e.g. Creyts and Schoof, 2009)

$$v \approx AN^n \ell, \quad (10)$$

so that the distance slipped during creep closure of a cavity in the lee side of an obstacle of height d is

$$\ell \approx \frac{du_s}{v} \approx \sqrt{\frac{du_s}{AN^n}}. \quad (11)$$

Substituting this and the undercooling expression from equation (7) into equation (9), while adopting a flow exponent of $n = 3$, gives (nominal values of physical constants are provided in Table 1)

$$h_0 \approx \frac{2C_p C_0 \rho_l}{(1 - \phi)(\rho_l - \rho_i) \mathcal{L}} \sqrt{\frac{\kappa}{\pi}} \left(\frac{Nd}{u_s A} \right)^{1/4} \approx \frac{(4.2 \times 10^{-6} \text{ m Pa}^{-1/4} \text{ s}^{-1/4})}{1 - \phi} \left(\frac{Nd}{u_s} \right)^{1/4}, \quad (12)$$

which is a relatively weak function of the primary variables that characterize the basal environment near the cavity, namely: N , d , and u_s . For example, with $\phi \ll 1$, $N = 10^5$ Pa and $d = 0.1$ m, $h_0 \approx 2$ mm when $u_s = 10$ m/a, and this thickness drops only slightly to $h_0 \approx 0.6$ mm when $u_s = 10^3$ m/a (with $N = 10^5$ Pa and $d = 0.1$ m) and increases slightly to $h_0 \approx 6$ mm when $N = 10^6$ Pa and $d = 1$ m (with $u_s = 10$ m/a). We emphasize that these values of h_0 should be regarded as order of magnitude estimates rather than precise predictions, particularly given the approximate treatment of the characteristic creep rate v in equation (10) and ℓ in equation (11).

Downstream Melting

Downstream of the cavity, some of the recently frozen-on water will melt. Upon reloading the basal interface on the opposite boundary of the drainage element, the temperature gradient is perturbed once again. Assuming a symmetrical unloading/reloading cycle so that the interface temperature drops abruptly by

153 ΔT and thereafter remains fixed for $x > \ell$ (see Fig. 1), the perturbation to the temperature gradient in
 154 the ice becomes (see Supplementary Information)

$$\nabla T \approx -\frac{\Delta T}{\sqrt{\pi\kappa}} \left(\sqrt{\frac{u_s}{x}} - \sqrt{\frac{u_s}{x-\ell}} \right), \quad (13)$$

155 which induces gradual melting so that the net ice-equivalent freeze-on thickness evolves according to

$$h = h_0 \left(\sqrt{\frac{x}{\ell}} - \sqrt{\frac{x}{\ell} - 1} \right) \approx \frac{h_0}{2} \sqrt{\frac{\ell}{x}}, \quad (14)$$

156 where the approximation on the right is valid for distances $x \gg \ell$. Importantly, even though the changes
 157 in interface temperature for this simple scenario are symmetrical — first increasing by ΔT at $x = 0$,
 158 then decreasing by ΔT at $x = \ell$ — the freezing and melting rates are not symmetrical. For example, the
 159 freeze-on thickness remains at $h = (\sqrt{2} - 1) h_0 \approx 0.4h_0$ after sliding to $x = 2\ell$ — a distance equivalent
 160 to the drainage element dimension beyond its downstream boundary. This asymmetry in phase change
 161 behavior arises because conductive transport ensures that the attenuated history of past temperature
 162 perturbations continues to exert an influence on the changes in heat flux imparted by each new jump in
 163 interface temperature — essentially, the thermal pulse produced by unloading continues to modify the
 164 heat transport even after reloading returns the interface temperature to the background level $T_{\text{pre-melt}}$.
 165 Our treatment assumes an initial steady-state profile that reaches $T_{\text{pre-melt}}$ at the basal interface, and
 166 subsequent perturbations to the temperature field forced by brief episodes with slightly warmer boundary
 167 temperatures result in net freeze-on as ice flows across and beyond drainage elements. It is worth noting
 168 that the supercooling described here is associated with motion of a cold sliding interface into contact with
 169 comparatively warmer water rather than the motion of comparatively colder water into contact with a
 170 warmer interface, as occurs during glaciohydraulic supercooling (e.g. Alley and others, 1998).

171 Idealized Cavity Sequences

172 A natural extension to this idealized treatment can be made by considering slip over cavities of dimension
 173 ℓ that are uniformly spaced by ℓ/ϕ , leading to a predicted freeze-on thickness immediately prior to the
 174 $J + 1$ st unloading of

$$h_{\min} \approx \frac{h_0 \sqrt{\phi}}{2} \sum_{j=1}^J j^{-1/2} \approx \frac{2C_p C_0 \rho_l N \phi}{\mathcal{L} (1 - \phi) (\rho_l - \rho_i)} \sqrt{\frac{\kappa x}{\pi u_s}}, \quad (15)$$

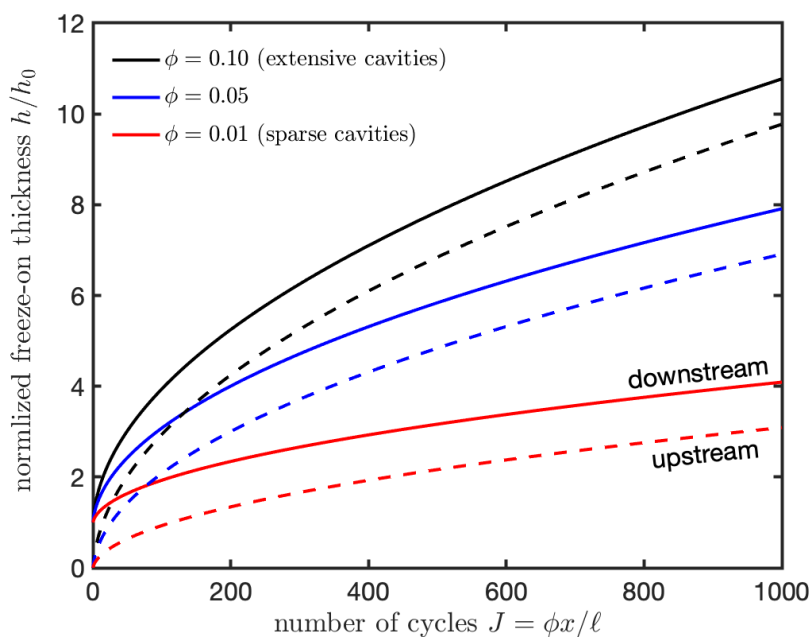


Fig. 2. Evolution of predicted freeze-on thickness with sliding over an evenly spaced sequence of identical cavities. Sliding distance is scaled by the cavity spacing $\phi^{-1}\ell$, with the values of ϕ noted in the legend. For a bed that contains more extensive cavities (high ϕ), there is proportionately less time for melt-out so h is larger for the same number of unload/reload cycles. Here, h is scaled by the characteristic dimension h_0 from equation (9). Dashed lines depict h_{\min}/h_0 , corresponding to predicted thicknesses on the upstream sides of cavities, while solid lines depict thicknesses h_{\max}/h_0 on the downstream sides of cavities. At other locations, h is expected to fall between these limits.

175 where the second approximation is valid for $J \gg 1$, or equivalently $x \gg \ell/\phi$. The next freeze-on episode
 176 enables the total thickness to reach

$$h_{\max} \approx h_{\min} + h_0 . \quad (16)$$

177 Figure 2 shows the evolution of minimum (dashed) and maximum (solid) freeze-on thicknesses predicted
 178 by equations (15) and (16) respectively, as a function of the sliding distance scaled to correspond with
 179 the number of complete unloading/reloading cycles. Net freeze-on increases gradually with the number of
 180 cycles and it also increases with the proportion of the bed occupied by macroscopic drainage elements ϕ .
 181 For example, with $N = 1$ MPa and $\ell = 1$ m, the total freeze-on thickness reaches approximately 10 cm
 182 after a sliding distance of 10 km when $\phi = 0.1$ and $u_s \approx 10$ m/a so that $h_0 \approx 1$ cm. Irrespective of cavity
 183 dimension ℓ , equation (15) indicates that h_{\min} is approximately proportional to the product $N\phi$ and the
 184 square root of the total sliding duration x/u_s , so two orders of magnitude more time would be required to
 185 grow h_{\min} to 1 m, and one order of magnitude lower $N\phi$ would reduce h_{\min} to 1 cm. However, the same

186 dynamic considerations that can cause ℓ to vary with basal conditions also make ϕ sensitive to N and
 187 u_s . For example, estimating the characteristic cavity size using equation (11) while treating the obstacle
 188 spacing as fixed suggests that the drainage fraction varies in the vicinity of some reference level ϕ_0 according
 189 to

$$\phi = \phi_0 \sqrt{\frac{u_s/u_{s0}}{N^n/N_0^n}}, \quad (17)$$

190 where N_0 and u_{s0} are the reference effective stress and sliding velocity for which $\phi = \phi_0$. Substituting this
 191 into equation (15) while taking $n = 3$ and assuming $\phi \ll 1$ leads to the functional behavior

$$h_{\min} \approx \frac{2C_p C_0 \rho_l \phi_0}{\mathcal{L}(\rho_l - \rho_i)} \sqrt{\frac{\kappa N_0^3 x}{\pi u_{s0} N}} \approx \left(0.4 \text{ m}^{1/2} \text{ Pa}^{1/2}\right) \phi_{\text{ref}} \sqrt{\frac{x}{N}}, \quad (18)$$

192 where the numerical factor on the right is valid when the reference drainage fraction $\phi_{\text{ref}} = \phi_0$ is defined
 193 using $N_0 = 10^5 \text{ Pa}$ and $u_{s0} = 10 \text{ m/a}$. The value of h_{\min} predicted by equation (18) is notably independent
 194 of sliding speed u_s since related potential changes in the time available for freeze-on over drainage elements
 195 are negated by increases in the drainage element fraction, according to the simple treatment leading to
 196 equation (17). Moreover, this particular model for the controls on drainage fraction implies that, despite
 197 the weak direct dependence of h_0 on effective stress in equation (12), h_{\min} actually decreases gradually with
 198 increased N since the nonlinearity in creep closure rate, described with Glen's flow law exponent $n = 3$,
 199 causes changes in N to affect ϕ more strongly than their linear influence on ΔT .

200 DISCUSSION AND CONCLUSIONS

201 The simple cases we consider here, with P and P_T in equation (4) both constant, represent a considerable
 202 idealization. In reality, both of these fields are likely to be heterogeneous, as are the temperature variations
 203 ΔT that drive freeze-on and melt-out during each unloading/reloading cycle. Commonly observed temporal
 204 variations in basal effective stress further complicate the balance of freezing and melting at the bed (e.g.
 205 Andrews and others, 2014; Huss and others, 2007; Iken and Bindschadler, 1986; Meierbachtol and others,
 206 2013; Rada and Schoof, 2018). All of these factors have the potential to leave their imprint on the basal ice
 207 and debris record. However, the relatively small variations that we predict for h_0 and h_{\min} in comparison
 208 with the much larger proportionate changes that we consider in characteristic basal parameters such as N
 209 and u_s , suggest that the dominant features of basal exchange may nevertheless be captured adequately by
 210 our idealized treatment. Extensions to consider more complicated and realistic scenarios with P and P_T
 211 both functions of time and space are not expected to introduce any significant conceptual hurdles.

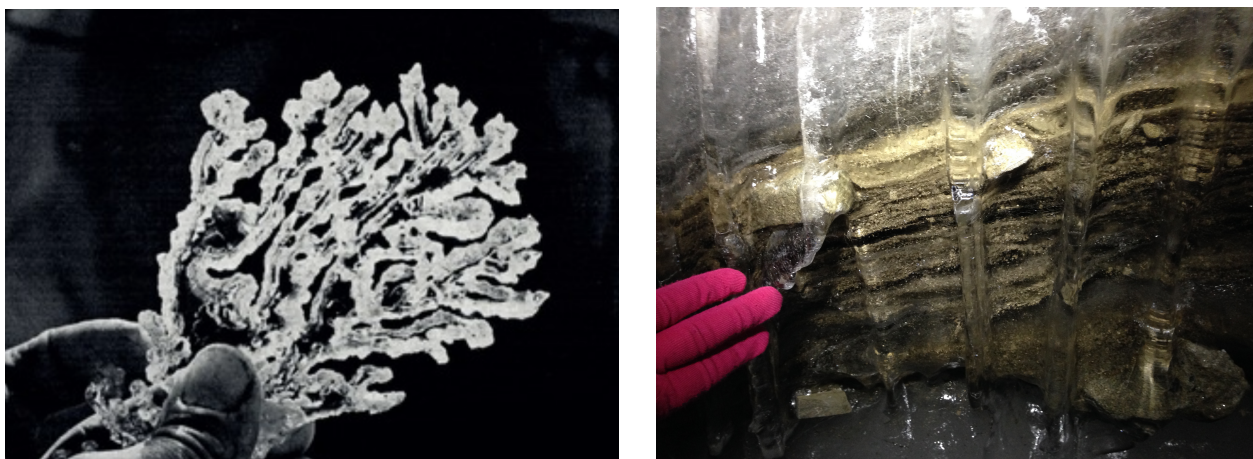


Fig. 3. Photos from the subglacial environment. A) Dendritic ice crystal recovered in 1967 from the wall of a drained subglacial cavity in marginal ice beneath Blue Glacier, WA (reprinted with permission from LaChapelle, 1968). B) Laminated facies photographed by KLR in 2014 beneath interior regions of Larsbreen glacier in Svalbard, accessed through the englacial drainage network and approximately 2.2km from the glacier terminus.

212 In situations where unloading occurs, liquid water at T_{drainage} is invariably exposed to a supercooled
 213 surface, initially at $T_{\text{pre melt}} < T_{\text{drainage}}$. Solidification in a dendritic growth habit may occur – whether
 214 downwards from the sliding glacial ice of a cavity roof (hinted at by reports of “regelation spicules” and
 215 other similar features seen in cavities beneath relatively shallow ice, e.g. Kamb and LaChapelle, 1964;
 216 Rea and Whalley, 1994; Theakstone, 1979; Vivian and Bocquet, 1973; LaChapelle, 1968, see Fig. 3A),
 217 or upwards as anchor ice growing on the mineral surfaces of a cold channel floor. The liquid water that
 218 flows through macroscopic drainage elements is expected to often contain suspended debris and indeed is
 219 sometimes observed to be quite turbid (e.g Rada and Schoof, 2018). These freezing styles may enhance
 220 the potential to incorporate mineral debris into the basal ice, particularly if mechanical disruption upon
 221 reloading (e.g. encapsulation in compacted dendritic layers or upwards particle displacement driven by
 222 debris–bed contact forces) acts to limit the efficiency of debris removal with small amounts of melt.

223 The approximate perturbation to the temperature gradient described by equation (8) does not include
 224 the effects of background heat flow (discussed briefly in the Supplementary Information), and neither
 225 have we accounted for bed-normal deformation (e.g. Knight, 1997; Sugden and others, 1987). Thicker
 226 basal ice sequences may develop if the average rate of conductive transport away from the basal interface
 227 is greater than the combined effects of geothermal heating and frictional work so that net freeze-on (i.e.
 228 congelation) takes place. In such circumstances, the basal mass exchange caused by the unloading/reloading
 229 cycles described here are expected to add and then subtract from the total evolving thickness of basal

ice layers. Other factors worthy of consideration include: i) the enhanced thermal conductivity of most common bed materials in comparison with liquid water (tending to focus geothermal heating away from drainage elements and towards premelted regions), ii) the absence of frictional work along the stress-free ice boundaries of macroscopic drainage elements (tending to favor slightly larger net freeze-on locally), iii) advective transport of heat with moving meltwater (potentially counteracting or even overwhelming the reduced heat input associated with an absence of frictional work), iv) longitudinal stress gradients that are often compressive in marginal regions (causing basal layers to thicken), and v) the potential for intergranular phase changes in temperate ice to reduce conductive heat transport (discussed further in the Supplementary Information). Without accounting for such complications, the simplest scenario to consider is one in which the background rate of freeze-on is constant over the entire glacier bed. To this is added the supercooling-induced freeze-on upon basal unloading and interaction with potentially turbid cavity waters, followed by subsequent melt-out upon re-establishment of ice–mineral stress transmission, as outlined above. Different rates and characters of debris entrainment are expected to accompany slow freezing at the equilibrium melting temperature from premelted films of water over mineral surfaces in comparison with that entrained during more rapid freezing along a supercooled and potentially dendritic interface with macroscopic drainage elements. The effects of subtle differences in freezing environment beneath different portions of the glacial bed are difficult to quantify (e.g. drainage system turbidity, bedrock debris cover and particle size distribution, background freeze-on rate, spatially and temporally varying effective stress), though some effects may be amenable to laboratory investigation. These differences may be preserved as distinct mm-scale layering involving diffuse debris concentrations of a similar nature to those termed “clotted ice”, “dispersed facies” or “laminated facies”, in reports of basal ice layers (e.g. Hubbard and others, 2009; Knight, 1997; Sugden and others, 1987). Further efforts to develop and test quantitative models that can reproduce specific features of observed basal debris distributions in particular settings hold promise for providing a window on the basal conditions sampled during flow.

The mechanism of debris entrainment introduced here is notably distinct from the ice-lensing phenomena that may sometimes accompany the growth of “frozen fringes” with much higher (i.e. > 50% by volume) debris concentrations beneath soft-bedded glaciers (e.g. Christoffersen and Tulaczyk, 2003; Meyer and others, 2018, 2019; Rempel, 2008), or any of the other most commonly recognized debris entrainment mechanisms (e.g. Alley and others, 1997). As noted previously (e.g. Rempel, 2011), the thicknesses of sediment-rich entrained layers produced by frozen-fringe modeling depends on lensing

260 criteria that can be related to a characteristic temperature offset, and for the low heat fluxes that
261 are typical of subglacial environments this makes it very difficult to use that mechanism to explain
262 mm-scale layering, such as that illustrated in Fig. 3B. Particularly intriguing observations of entrained
263 basal debris deep in the interior of Kamb Ice Stream are captured in borehole video accessible
264 through Engelhardt (2013, <https://nsidc.org/data/nsidc-0528/versions/1/documentation>). In principal,
265 entrainment by glaciohydraulic supercooling can result in diffuse debris contents and fine-scale layering,
266 but this mechanism is normally invoked to describe behavior on adverse bed slopes (e.g. Alley and others,
267 1998), making it difficult to reconcile with the ubiquity of debris observations. While noting that several
268 other potential mechanisms have been proposed and likely dominate in some environments, we suggest
269 that remnants of the basal mass exchange processes introduced here may often be preserved as dispersed
270 and laminated facies within basal ice layers.

271 ACKNOWLEDGEMENTS

272 We would like to thank Lauren Andrews and Mauro Werder for sharing basal temperature records that
273 illuminated a serious misconception held by AWR, and Gwenn Flowers for several discussions that helped
274 propel this work forward. Revisions benefited from comments, questions, assertions and suggestions by
275 Florent Gimbert, two anonymous reviewers, and the Scientific Editor, Sergio Faria. Financial support
276 came from NSF-1603907 and the University of Oregon.

277 REFERENCES

- 278 Alley RB, Cuffey K, Evenson E, Strasser J, Lawson D and Larson G (1997) How glaciers entrain and transport basal
279 sediment: physical constraints. *Quaternary Science Reviews*, **16**(9), 1017–1038
- 280 Alley RB, Lawson DE, Evenson EB, Strasser JC and Larson GJ (1998) Glaciohydraulic supercooling: a freeze-on
281 mechanism to create stratified, debris-rich basal ice: II. Theory. *Journal of Glaciology*, **44**(148), 563–569
- 282 Andrews LC, Catania GA, Hoffman MJ, Gulley JD, Lüthi MP, Ryser C, Hawley RL and Neumann TA (2014) Direct
283 observations of evolving subglacial drainage beneath the Greenland Ice Sheet. *Nature*, **514**(7520), 80–83
- 284 Bottomley JT (1872) Melting and regelation of ice. *Nature*, **5**, 185
- 285 Carslaw HS and Jaeger JC (1959) *Conduction of Heat in Solids*. Oxford: Clarendon Press, 2nd ed.
- 286 Christoffersen P and Tulaczyk S (2003) Response of subglacial sediments to basal freeze-on 1. Theory and comparison
287 to observations from beneath the West Antarctic Ice Sheet. *Journal of Geophysical Research: Solid Earth*, **108**(B4)

- 288 Creyts TT and Schoof C (2009) Drainage through subglacial water sheets. *J. Geophys. Res.*, **114**(F04008), 1–18 (doi:
289 10.1029/2008jf001215)
- 290 Cuffey KM and Paterson WSB (2010) *The Physics of Glaciers (Fourth Edition)*. ISBN 9780123694614, Elsevier
- 291 Dash J (1989) Thermomolecular pressure in surface melting: motivation for frost heave. *Science*, **246**(4937), 1591–
292 1593
- 293 Dash JG, Rempel AW and Wettlaufer JS (2006) The physics of premelted ice and its geophysical consequences. *Rev.*
294 *Mod. Phys.*, **78**(3), 695 (doi: 10.1103/RevModPhys.78.695)
- 295 Drake L and Shreve R (1973) Pressure melting and regelation of ice by round wires. *Proceedings of the Royal Society*
296 *of London A*, **332**(1588), 51–83
- 297 Engelhardt H (2013) Videos of basal ice in boreholes on the kamb ice stream in west antarctica, u.s. antarctic program
298 (usap) data center (doi: 10.7265/N5028PFH)
- 299 Flowers GE (2015) Modelling water flow under glaciers and ice sheets. *Proceedings of the Royal Society A*, **471**(2176),
300 20140907
- 301 Fowler A (2010) Weertman, Lliboutry and the development of sliding theory. *Journal of Glaciology*, **56**(200), 965–972
- 302 Gilpin R (1979) A model of the “liquid-like” layer between ice and a substrate with applications to wire regelation
303 and particle migration. *Journal of Colloid and Interface Science*, **68**(2), 235–251
- 304 Hubbard B, Cook S and Coulson H (2009) Basal ice facies: a review and unifying approach. *Quaternary Science*
305 *Reviews*, **28**(19-20), 1956–1969
- 306 Huss M, Bauder A, Werder M, Funk M and Hock R (2007) Glacier-dammed lake outburst events of Gornersee,
307 Switzerland. *Journal of Glaciology*, **53**(181), 189–200
- 308 Iken A and Bindschadler RA (1986) Combined measurements of subglacial water pressure and surface velocity of
309 Findelengletscher, Switzerland: conclusions about drainage system and sliding mechanism. *Journal of Glaciology*,
310 **32**(110), 101–119
- 311 Israelachvili JN (2011) *Intermolecular and Surface Forces*. Academic press
- 312 Kamb B (1970) Sliding motion of glaciers: theory and observation. *Rev. Geophys.*, **8**(4), 673–728 (doi:
313 10.1029/RG008i004p00673)
- 314 Kamb B (1987) Glacier surge mechanism based on linked cavity configuration of the basal water conduit system.
315 *Journal of Geophysical Research: Solid Earth*, **92**(B9), 9083–9100
- 316 Kamb B and LaChapelle E (1964) Direct observation of the mechanism of glacier sliding over bedrock. *Journal of*
317 *Glaciology*, **5**(38), 159–172
- 318 Kamb WB (1961) The thermodynamic theory of nonhydrostatically stressed solids. *Journal of Geophysical Research*,
319 **66**(1), 259–271

- 320 Knight PG (1997) The basal ice layer of glaciers and ice sheets. *Quaternary Science Reviews*, **16**(9), 975–993
- 321 LaChapelle E (1968) Stress-generated ice crystals in a nearly isothermal two-phase system. *Journal of Glaciology*,
322 **7**(50), 183–198
- 323 Lliboutry L (1968) General theory of subglacial cavitation and sliding of temperate glaciers. *Journal of Glaciology*,
324 **7**(49), 21–58
- 325 Meierbachtol T, Harper J and Humphrey N (2013) Basal drainage system response to increasing surface melt on the
326 Greenland Ice Sheet. *Science*, **341**(6147), 777–779
- 327 Meyer CR, Downey AS and Rempel AW (2018) Freeze-on limits bed strength beneath sliding glaciers. *Nature*
328 *Communications*, **9**(1), 1–6
- 329 Meyer CR, Robel AA and Rempel AW (2019) Frozen fringe explains sediment freeze-on during Heinrich events. *Earth*
330 *and Planetary Science Letters*, **524**, 115725
- 331 Nye J (1967) Theory of regelation. *Philosophical Magazine*, **16**(144), 1249–1266
- 332 Nye JF (1969) A calculation on the sliding of ice over a wavy surface using a Newtonian viscous approximation. *Proc.*
333 *R. Soc. Lond. A*, **311**(1506), 445–467 (doi: 10.1098/rspa.1969.0127)
- 334 Paterson M (1973) Nonhydrostatic thermodynamics and its geologic applications. *Reviews of Geophysics*, **11**(2),
335 355–389
- 336 Rada C and Schoof C (2018) Subglacial drainage characterization from eight years of continuous borehole data on a
337 small glacier in the Yukon Territory, Canada. *The Cryosphere*, **12**, 2609–2636
- 338 Rea BR and Whalley WB (1994) Subglacial observations from øksfjordjøkelen, north Norway. *Earth Surface Processes*
339 *and Landforms*, **19**(7), 659–673
- 340 Rempel AW (2008) A theory for ice-till interactions and sediment entrainment beneath glaciers. *J. Geophys. Res.*,
341 **113**(F1), ISSN 2156-2202 (doi: 10.1029/2007JF000870), f01013
- 342 Rempel AW (2011) Microscopic and environmental controls on the spacing and thickness of segregated ice lenses.
343 *Quaternary Research*, **75**(2), 316–324
- 344 Rempel AW and Meyer CR (2019) Premelting increases the rate of regelation by an order of magnitude. *Journal of*
345 *Glaciology*, **65**(251), 518–521
- 346 Schoof C (2005) The effect of cavitation on glacier sliding. *Proc. R. Soc. Lond. Ser. A*, **461**(2055), 609–627 (doi:
347 10.1098/rspa.2004.1350)
- 348 Sekerka RF and Cahn JW (2004) Solid–liquid equilibrium for non-hydrostatic stress. *Acta Materialia*, **52**(6), 1663–
349 1668
- 350 Sugden D, Knight P, Livesey N, Lorrain R, Souchez R, Tison JL and Jouzel J (1987) Evidence for two zones of debris
351 entrainment beneath the Greenland ice sheet. *Nature*, **328**(6127), 238–241

- 352 Telford J and Turner J (1963) The motion of a wire through ice. *Philosophical Magazine*, **8**(87), 527–531
- 353 Theakstone WH (1979) Observations within cavities at the bed of the glacier østerdalsisen, Norway. *Journal of*
354 *Glaciology*, **23**(89), 273–281
- 355 Thompson A, Iverson NR and Zoet L (2020) Controls on subglacial rock friction: Experiments with debris in
356 temperate ice. *Journal of Geophysical Research: Earth Surface*, e2020JF005718
- 357 Vivian R and Bocquet G (1973) Subglacial cavitation phenomena under the glacier d'Argentière, Mont Blanc, France.
358 *Journal of Glaciology*, **12**(66), 439–451
- 359 Weertman J (1957) On the sliding of glaciers. *J. Glaciol.*, **3**(21), 33–38 (doi: 10.3198/1957JoG3-21-33-38)
- 360 Wettlaufer JS and Worster MG (2006) Premelting dynamics. *Ann. Rev. Fluid Mech.*, **38**(1), 427–452 (doi:
361 10.1146/annurev.fluid.37.061903.175758)

For Peer Review